20th Australasian Fluid Mechanics Conference
Perth, Australia
5-8 December 2016

Experimental and Numerical Investigation of the Impact of Gas Channel Configuration on the Performance of a Small Scale PEM Fuel Cell

Murphy K.K. Lai[1], Xiang Wu[1], Sherman C.P. Cheung[1], John Andrews[1]

[1]School of Engineering, RMIT University, Bundoora VIC 3082, Australia

Abstract

With the ever tightening greenhouse gas emission target, it is envisioned that the Proton Exchange Membrane (PEM) fuel cells using hydrogen as fuel could be the next generation environmental friendly fuel alternative. This paper presents the preliminary findings of our recent experimental and numerical investigation of the performance of a small scale PEM fuel cell. A typical small scale PEM fuel cell with dimensions of 27mm by 30mm has been constructed. Parallel gas channels with a common header configuration was adopted for supplying hydrogen and air to the gas diffusion layers of the PEM fuel cell. The performance of the PEM fuel cell was investigated and the corresponding V-I curve was measured from the experiment. In addition, a three-dimensional numerical model for the PEM fuel cell has also been developed using the ANSYS Fuel Cell Module and been adopted to investigate the overall fuel cell performance. Governing equations of the numerical model take into account the 'multiphysics' occurring in the PEM fuel cell including fluid flow in channels, electrochemical reactions at the catalyst layers, and their associated heat and mass transfer within the cell. The impact on the reactants delivery on current density were discussed through numerical results from which it also revealed the problem of water removal and the possible modelling challenge in future.

Introduction

Fuel cells are electrochemical devices that covert the energy of a fuel directly into electricity. The fuel may include hydrogen, natural gas or other hydrocarbons. Types of fuel cells available include alkaline (AFC), phosphoric acid (PAFC), molten carbonate (MCFC), solid oxide (SOFC) and polymer electrolyte membrane (PEM) fuel cells [4] that provide electricity without polluting the environment. Among all types, PEM fuel cell operates at significantly lower temperature than other types of fuel cells and has been regarded as a strong candidature for the future power generation [5]. The technology of PEM fuel cell has drawn the most attention also because of its simplicity, viability, quick start-up, and its application can range from powering a cell phone to a locomotive [8].

The general concept of the PEM fuel cell operation is characterised as gas-mixture transport and transportation of species by electrochemical reactions. Several experimental investigations [6, 7] have been conducted towards the gas channel configurations, the delivery of reactants and various cell performance parameters as well as the problems on water and heat removal. The global validation in terms of the V-I curve is generally recognised as the benchmark validation tool for numerical study of PEM fuel cells [9]. Such validations usually provide a combined effect of the macroscopic performance of the fuel cells without thoroughly understanding the microscopic behaviour of various components of the fuel cell because of the inherited complexity of the fuel cells, feasibility and accuracy in measuring precisely the behaviour with microscopic sized products and its generic criterion of cost worthiness.

On the other hand, numerical investigations have also been conducted to study the effect of humidity, temperature distribution, single-phase and two-phase transports, effect of diffusion resistance of PEM fuel cells [2, 3, 10]. Nevertheless, very few of the previous works addressed the aforementioned coupling effect, especially on the high power side of the PEM fuel cell which is usually governed by the mass transport losses. Studies showed that the loss in reactant concentration greatly influences the cell performance [1, 11, 13]. [1] also asserted that the phenomena occurring within a PEM fuel cell can generally be represented by the solution of conservation equations of mass, momentum, energy, species and current transport.

The present study aims to grasp an in-depth understanding on the multiphysics of the performance of a typical small scale fuel cell which might encounter large variations between experimental measurements and numerical investigations. Such multiphysics understanding could provide insights for the problems of reactant flows, electrochemical stability and water and heat management which serve as the basis for future PEM fuel cell design.

Experimental Setup and Numerical Methodology

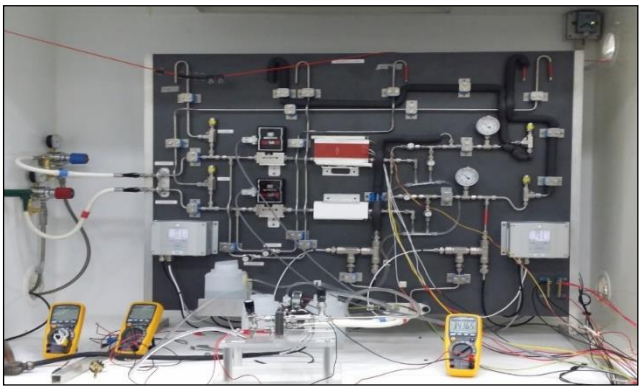

Figure 1. Experimental setup for the present investigation

A experimental rig fitted with separate mass flow meters, heating blocks, humidifiers, humidity meters and temperature measurement devices for both hydrogen and oxygen gases has been constructed. Two separate pressure relief valves are fitted in each gas line of the rig, which ensure gas pressure at the entry of fuel cell will not be more than 1 bar. A relatively high pressure (0.9 bar gauge, primarily for air/oxygen) to ensure sufficient reactants are available to the cathode. The PEM fuel cell is maintained at a reasonably high temperature (of approx. 55 ℃) to ensure liquid water retention is reduced for avoid water flooding problem, together with assistance in increasing the kinetics of the reaction. No pre-heating of input gases prior to their entry into the cell and gas flow rates ranging between 50 to 80 $mLmin^{-1}$. Medium relative humidity of approximately 40 and 70 %RH for air and hydrogen respectively.

For the numerical simulation, the AYSYS FLUENT Fuel Cell Module 14.5 was adopted in the present study for resolving the electrochemical reactions of the PEM Fuel Cell. The governing equations for the numerical simulations are conservation of mass, momentum, energy, species and charge.

Conservation of mass equation:

$$\frac{\partial \rho}{\partial t} + \nabla \cdot (\rho v) = 0 \quad (1)$$

where ρ is the density, kgm^{-3}; v is the velocity vector, ms^{-1}

Conservation of momentum equation:

$$\frac{\partial (\rho v)}{\partial t} + \nabla \cdot (\rho v v) = -\nabla p + \nabla \cdot \left(\mu^{eff} \nabla v\right) + S_m \quad (2)$$

where p is the fluid pressure; Pa; μ^{eff} is the mixture average viscosity; kgm^{-1}s^{-1}; S_m is the momentum source term.

Conservation of energy equation:

$$\left(\rho C_p\right)_{eff} \frac{\partial T}{\partial t} + \left(\rho C_p\right)_{eff} (v \cdot \nabla T) = \nabla \cdot \left(k_{eff} \nabla T\right) + S_e \quad (3)$$

where C_p is mixture-averaged specific heat capacity, Jkg^{-1}K^{-1}; T is the temperature, K; k is the thermal conductivity, Wm^{-1}K^{-1}; S_e is the energy source term.

Conservation of species equation:

$$\frac{\partial (\epsilon \rho X_i)}{\partial t} + \nabla \cdot (v \epsilon \rho X_i) = \nabla \cdot \left(\rho D_i^{eff} \nabla X_i\right) + S_{s,i} \quad (4)$$

where X_i is the mass fraction of gas species; $S_{s,i}$ is the source or sink terms for the species.

Conservation of charge equation:

$$\nabla \cdot \left(k_s^{eff} \nabla \emptyset_s\right) = S_{\emptyset s} \quad (5)$$

$$\nabla \cdot \left(k_m^{eff} \nabla \emptyset_m = S_{\emptyset m}\right) \quad (6)$$

where k_s^{eff} is the electrical conductivity in the solid phase, Scm^{-1}; k_m^{eff} is the ionic conductivity in the ionomer phase, Scm^{-1}; $\emptyset_s$ is the solid phase potential, V; $\emptyset_m$ is the electrolyte phase potential, V; $S_\emptyset$ is the source term representing volumetric transfer current at the anode catalyst layer $S_{\emptyset s} = -j_a$ and $S_{\emptyset m} = j_a$; at the cathode catalyst layer $S_{\emptyset s} = j_c$ and $S_{\emptyset m} = -j_c$ and $S_\emptyset = 0$ elsewhere.

The general definitions for the source terms are:

$$R_{an} = \left(\zeta_{an} j_{an}^{ref}\right) \left[\frac{[A]}{[A]_{ref}}\right]^{\gamma_{an}} \left(e^{\alpha_{an} F \frac{\eta_{an}}{RT}} - e^{-\alpha_{cat} F \frac{\eta_{an}}{RT}}\right) \quad (7)$$

$$R_{cat} = \left(\zeta_{cat} j_{cat}^{ref}\right) \left[\frac{[C]}{[C]_{ref}}\right]^{\gamma_{cat}} \left(-e^{\alpha_{an} F \frac{\eta_{cat}}{RT}} + e^{-\alpha_{cat} F \frac{\eta_{cat}}{RT}}\right) \quad (8)$$

where j^{ref} is the reference exchange current density per active surface area, Am^{-2}; ζ is the specific active surface area, m^{-1}; [], []$_{ref}$ are the local species concentration and reference value respectively, kmolm^{-3}; γ is the concentration dependence; α is transfer coefficient; F is the Faraday constant; [A] represents the H_2 in the anode side; [C] represents the O_2 in the cathode side.

Heat source equation:

$$S_h = h_{react} - R_{an,cat} \eta_{an,cat} + I^2 R_{ohm} + h_L \quad (9)$$

where h_{react} is the net enthalpy change due to the electrochemical reactions; $R_{an,cat}\eta_{an,cat}$ is the product of the transfer current and the overpotential in the anode or the cathode triple-phase boundaries; R_{ohm} is the ohmic resistivity of the conducting media; and h_L is enthalpy change due to condensation/vaporization of water. Liquid water formation uses the saturation model based on [12].

With reference to the experimental fuel cell, a three-dimensional computational PEM fuel cell model was constructed for simulation. A computational mesh consists of a total 3,534,043 nodes was generated to discretise every layer of the fuel cell. To compare with the experimental measurements, steady state simulations were carried out and the boundary conditions for the gas channels were specified based on the experimental conditions. Material properties of each layer (e.g. density, specific heat capacity, thermal and electrical resistance) are assumed to be constant. Figure 2.1 & 2.2 show the visualization of the computational model and corresponding mesh distribution of the computational domain. Boundary conditions and properties of each layer are also tabulated in Table 1.

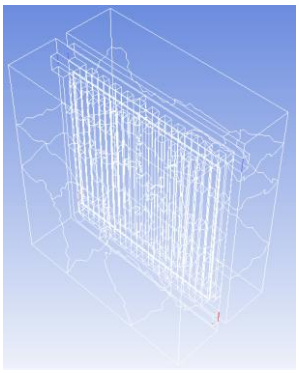

Figure 2.1 Computational model.

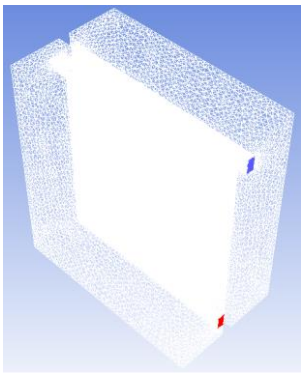

Figure 2.2 Mesh distribution of the computational domain.

	Density, kgm^{-3}	Specific heat capacity, kJkg^{-1}K^{-1}	Thermal conductivity, Wm^{-1}K^{-1}	Electrical conductivity, 1ohm^{-1}m^{-1}
Electrolyte	1968.5	2000	2	1e-16
Anode catalyst	2719	871	10	5000
Cathode catalyst	2719	871	10	5000
Anode GDL	377	871	10	267059
Cathode GDL	1351.8	520	21.9	2.38e6
Collectors	8000	500	16.3	1.35e6

Table 1. Properties of PEM fuel cell layers

The height of channels is 1mm while the widths of headers and straight parallel channels are 2mm and 1mm respectively. The dimensions of flow channels are 1mm by 1mm, the thickness of cathode gas diffusion layer, cathode catalyst, membrane, anode catalyst and anode gas diffusion layers are 0.1 mm, 0.01 mm, 0.03 mm, 0.01 mm and 0.454 mm respectively. Some other physical parameters are listed in Table 2:

Operating pressure	101,325 Pa
Velocities of anode and cathode flow channels	0.37, 6 ms^{-1}
Porosities of GDL_a and GDL_c	0.63, 0.7
Porosities of catalyst layers	0.5
Mass fractions of h_2 and O_2	0.96, 0.21
Operating temperatures at anode and cathode	294, 322 K
Open circuit voltage	1.1 V

Table 2. Physical parameters for numerical simulations.

Results and Discussion

Model Validation for the Performance of the Fuel Cell

The numerical prediction is firstly validated against the experimental measurements. Figure 3 shows the comparison of the predicted and measured performance (i.e. V-I curve) of the small-

scale PEM fuel cell. As depicted, the predicted performance is in good agreement with experimental data. Particular attention is directed toward the comparison at the activation and the ohmic loss region. As shown in the figure, the numerical model has successfully captured the first drop of the voltage due to the activation loss as well as the linear voltage drop against current due the ohmic loss mechanism. On the other hand, noticeable errors were found in the mass transport loss region where the transfer of liquid water or vapour could be inaccurately modelled in the simulation.

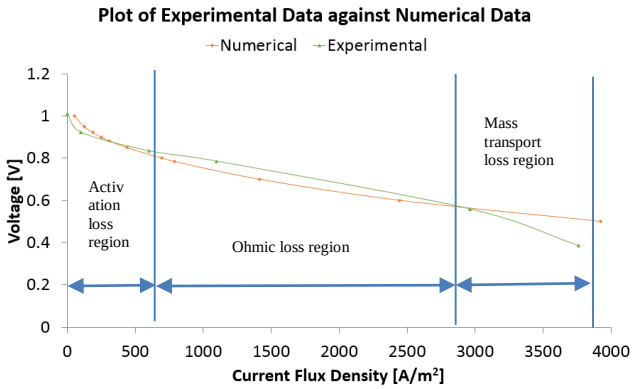

Figure 3. Validation plot of numerical and experimental data.

The following analyses mainly focus on the comparison between low voltage (0.38V) high power and high voltage (0.92V) low power scenarios and its associated water and heat distributions in the cathode catalyst layer.

Velocity Profiles at Flow Channels

Figures 4.1 & 4.2 shows the velocity distribution of the parallel straight channels in the both anode and cathode side. The flows are essentially co-flow between anode and cathode channels. In both cases, high velocities dominate at the inlet and outlet area. The velocities gradually diminish at the headers from the inlets as the volume of flow diversifies towards the branches of straight channels while the velocities progressively increase at the headers towards the outlets as the volume of flow accumulates from the branches of straight channels. While in both flow channels, one could notice that the minimum velocities are found at the mid branches; showing the non-uniformity of the gas flow in channels.

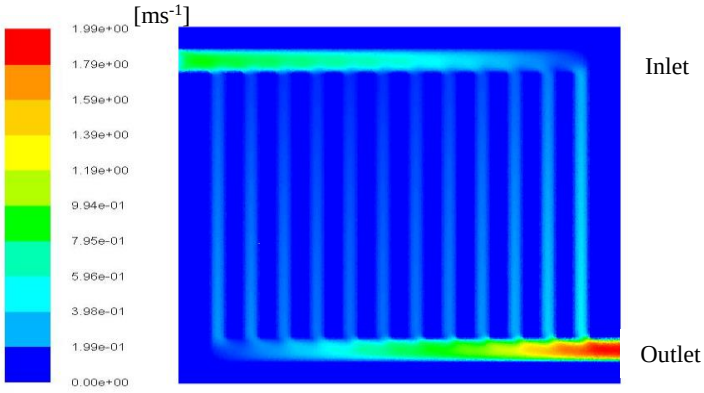

Figure 4.1. Velocity contour of H_2 at anode channels at 0.38V

Reactants Delivery at Cathode Catalyst Layer

Figures 5.1 & 5.2 shows the mass fraction distributions of the reactants (i.e. O_2) in the cathode catalyst layer with parallel straight channels flows inside cathode flow channels. The anode flow channels exhibit a non-uniform distributions at headers and parallel straight channels which corresponds to its non-uniformity in velocity profiles. The lower concentration in straight channels is possibly caused by the reduced velocity and thus enhanced diffusion to the anode gas diffusion layer. The similarity between the delivery of reactant and its velocity profile can also be found at the cathode channels with enhanced diffusion to cathode gas diffusion layer at correspondingly reduced velocity. The header near the inlet has significantly higher mass fraction than the header close to the outlet while the middle flow channels displayed the maximum diffusion in the whole set of cathode flow channels. The higher retention of O_2 in the high voltage case is possibly due to the lower of reaction rate in the catalyst layer.

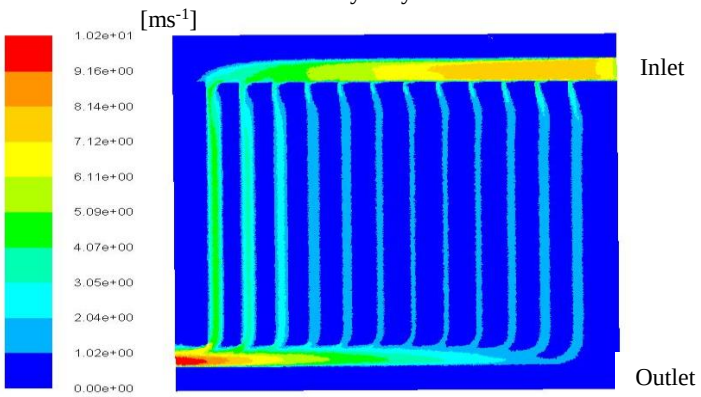

Figure 4.2. Velocity contour of air at cathode channels at 0.38V

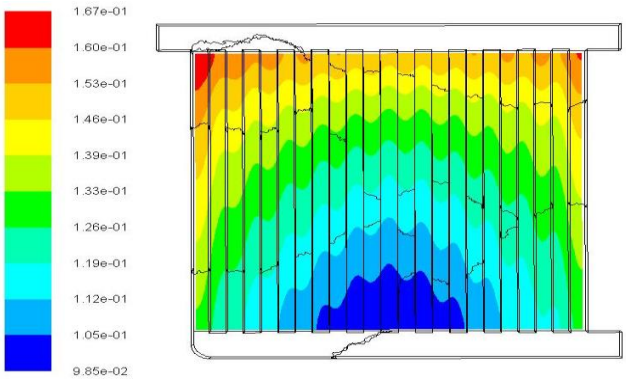

Figure 5.1. Mass fraction of O_2 at cathode catalyst at 0.38V

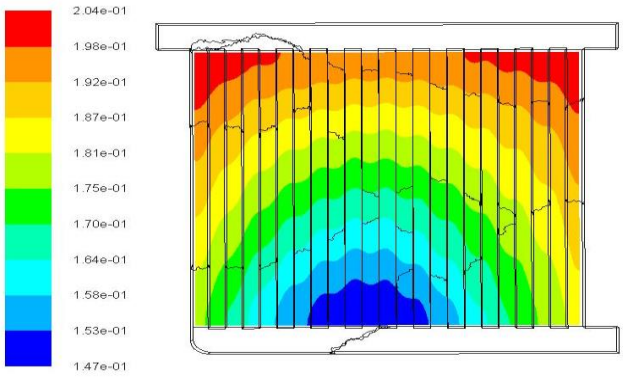

Figure 5.2. Mass fraction of O_2 at cathode catalyst at 0.92V

Current Density at Cathode Catalyst Layer

The current densities (Figures 6.1) tends to concentrate near the inlet header and then decrease gradually down the parallel straight channels. The dome-shaped current density distribution shows the lowest power at the mid channels which corresponds to its low velocity distribution. Such low power output is caused by the ineffective delivery of reactants to the channels and subsequently affecting the amount of reactants diffused to the catalyst layer for reactions. Besides, the present setting shows a similar current density pattern for the higher power output at low voltage (0.38V) case and a lower power output at high voltage (0.92V) case with a difference in magnitude of 2. However, the blue region clearly

indicates the poor performance of the chemical reaction which can be related to the insufficient reactant delivered at low velocity.

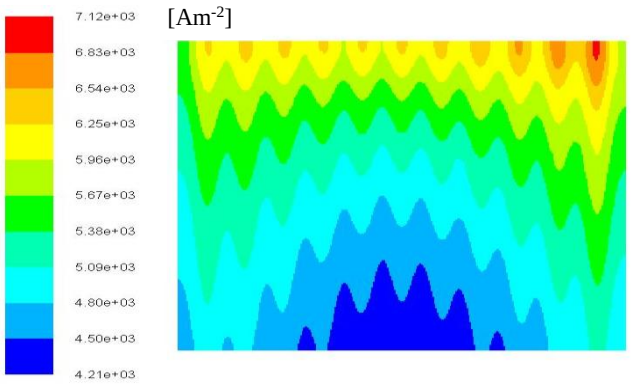

Figure 6.1. Current density distribution at cathode catalyst at 0.38V

Water Distribution at Cathode Catalyst Layer

Figures 7.1 & 7.2 displays the water distribution at the cathode catalyst layer. A high mass fraction of water dominates at the inlet header and then decreases gradually downwards to the outlet headers. The pattern of distribution matches well with the power distribution. The difference in mass fraction between the low voltage and the high voltage cases is less than 2 times the lower one. The amount of water increment displays a high relationship with the amount of reactants successfully delivered to the catalyst and in other words, high power output tends to have more water accumulation and such water accumulation is generally recognised as a hindrance to the reactant delivery. As the present investigation did not take into account of the ways of water removal through geometrical consideration or material advancement so that the validation curve shows an increasing discrepancy at mass transport loss region.

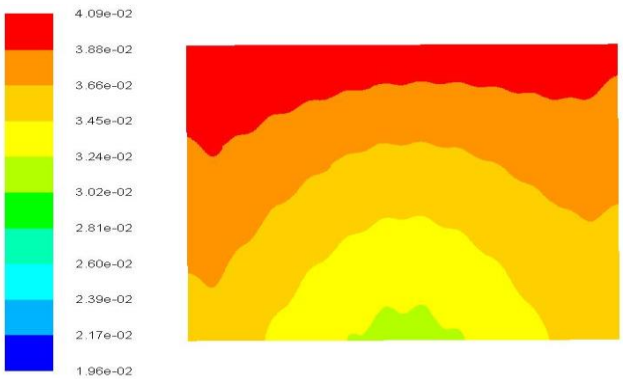

Figure 7.1. Mass fraction of H_2O at cathode catalyst at 0.38V

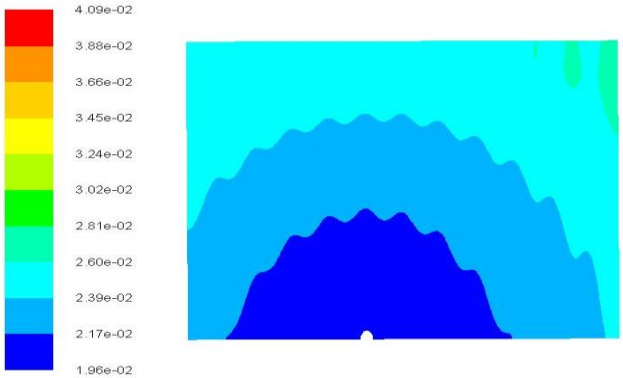

Figure 7.2. Mass fraction of H_2O at cathode catalyst at 0.92V

Conclusions

The current study reviewed the experimental results, numerical development and their interconnected validations. Those practically immeasurable contents from experimental study could gain more in-depth knowledge with the help of numerical prediction. Therefore, merely using the global validation on the V-I curve might not be so effective to formulate a plan in fuel cell optimisation. The present investigation preliminarily concluded that there is a high relationship among velocity profiles, current densities, water distributions and above all, the dominating factor is said to be the amount of reactants which can be successfully delivered to the reaction site. The degree of reactions eventually determined the power and water output to the PEM fuel cell, Future investigations would review the possible drawback of gas channel configurations to maximise the reactant delivery at low reaction region and to enhance the water removal at low voltage high power operation.

References

[1] Barbir, F., PEM Fuel Cells - Theory and Practice, 2013, *Elsevier*.

[2] Berning, T. & Djilali, N., Three-Dimensional Computational Analysis of Transport Phenomena in a PEM Fuel Cell-A Parametric Study, *J. of Power Sources*, **124** (2), 2003, 440-452.

[3] Dutta, S., Shimpalee, S. & Van Zee, J.W., Numerical Prediction of Mass-Exchange Between Cathode and Anode Channels in a PEM Fuel Cell, *Int. J. of Heat & Mass Trans*, **44**(11), 2001, 2029-2042.

[4] Hamilton, P.J. & Pollet, B.G., Polymer Electrolyte Membrane Fuel Cell (PEMFC) Flow Field Plate: Design, Materials and Characterisation. *Fuel Cell*, **10** (4), 2010, 489-509

[5] Hirschenhofer, J.H., Stauffer, D.B. & Engleman, R.R., Fuel Cells: A Handbook.

[6] Iranso, A., Munoz, M., Lopez, E., Pino, J. & Rosa, F., Experimental Fuel Cell Performance Analysis Under Different Operating Conditions and Bipolar Plate Designs, *Int. J. of Hydro. Energy*, **35**, 2010, 11437-11447.

[7] Ju, H. & Wong, C.Y., Experimental Validation of a PEM Fuel Cell Model by Current Distribution Data, *J. of Electrochem. Society*, **151** (11), 2004, A1594.

[8] Larminie, J. & Dicks, A., Fuel Cell Systems Explained, **2nd Edition**, *John Wiley & Sons, Inc.*

[9] Lum, K.W. & McKuirk, J.J., 2D and 3D Modelling of a PEMFC Cathode with Interdigitated Gas Distributors, *J. of Electrochem. Society*, **152** (4), 2005, A811-A817.

[10] Meng, H., & Wang, C.Y., Large-Scale Simulation of Polymer Electrolyte Membrane Fuel Cells by Parallel Computing, *Chem. Engg Sci.*, **59** (16), 2004, 3331-3343.

[11] Natarajan, D. & Nguyen, T.V., A Two-Dimensional, Two-Phase, Multicomponent, Transient Model for the Cathode of a Proton Exchange Membrane Fuel Cell Using Conventional Gas Distributors, *J. of Electrochem. Society*, **148** (12), 2001, A1324-A1335.

[12] Nguyen, Trung, V., Modelling Two-phase Flow in the Porous Electrode pf Proton Exchange Membrane Fuel Cells Using the Interdigitated Flow Fields, *Tutorial in Electrochem. Engg Mathe. Modelling*, **99** (14), 1999, 222-241.

[13] Shimpalee, S., Dutta, S., Lee, S.K. & Van Zee, J.W., Effect of Humidity on PEM Fuel Cell Performance: Part II-Numerical Simulations, *ASME Publ.*, **364**, 1999, 367-374.